Nano Research
https://doi.org/10.1007/s12274-018-2096-7
Research Article
ISSN 1998-0124
CN 11-5974/O4

MoS_2/C/C nanofiber with double-layer carbon coating for high cycling stability and rate capability in lithium-ion batteries

Hao Wu[1], Chengyi Hou[1], Guozhen Shen[3], Tao Liu[4], Yuanlong Shao[2] (✉), Ru Xiao[1] (✉), and Hongzhi Wang[1]

[1] *State Key Laboratory for Modification of Chemical Fibers and Polymer Materials, College of Materials Science and Engineering, Donghua University, Shanghai 201620, China*
[2] *Cambridge Graphene Center, Department of Engineering, University of Cambridge, Cambridge, CB3 0FA, UK*
[3] *State Key Laboratory for Superlattices and Microstructures, Institute of Semiconductors, Chinese Academy of Sciences, Beijing 100083, China*
[4] *Chemistry Department, University of Cambridge, Lensfield Road, Cambridge CB2 1EW, UK*

Received: 19 February 2018
Revised: 17 April 2018
Accepted: 12 May 2018

KEYWORDS
electrospinning,
fiber electrode,
molybdenum disulfide,
lithium-ion battery

ABSTRACT

MoS_2 has attracted a lot of interest in the field of lithium-ion storage as an anode material owing to its high capacity and two-dimensional (2D)-layer structure. However, its electrochemical properties, such as rate capability and cycling stability, are usually limited by its low conductivity, volume variation, and polysulfide dissolution during lithiation/delithiation cycling. Here, a designed two-layer carbon-coated MoS_2/carbon nanofiber (MoS_2/C/C fiber) hybrid electrode with a double-layer carbon coating was achieved by a facile hydrothermal and subsequent electrospinning method. The double carbon layer (inner amorphous carbon and outer carbon fiber) shells could efficiently increase the electron conductivity, prevent the aggregation of MoS_2 flakes, and limit the volume change and polysulfide loss during long-term cycling. The as-prepared MoS_2/C/C fiber electrode exhibited a high capacity of up to 1,275 mAh/g at a current density of 0.2 A/g, 85.0% first cycle Coulombic efficiency, and significantly increased rate capability and cycling stability. These results demonstrate the potential applications of MoS_2/C/C fiber hybrid material for energy storage and may open up a new avenue for improving electrode energy storage performance by fabricating hybrid nanofiber electrode materials with double-layer carbon coatings.

1 Introduction

MoS_2 is one of the typical two-dimensional (2D) transition-metal dichalcogenides (TMDs), with a layered structure loosely held together by the Van der Waals interaction. MoS_2 exhibits a unique

Address correspondence to Yuanlong Shao, ys461@cam.ac.uk; Ru Xiao, xiaoru@dhu.edu.cn

graphite-like structure in which the Mo hexagonal layers are sandwiched by two S layers, and each layer is bonded by strong covalent bonds (Mo–S) [1–3]. Due to its unique structure, MoS_2 demonstrates a variety of physical and chemical properties, such as photoluminescence, a bulk indirect band gap of 1.3 eV (which is similar to silicon), and excellent electrochemical performance for applications in photo/electrocatalysts, energy storage, and conversion devices [4–8]. Because of the weak interlayer interaction and large interlayer distance of 0.65 nm between each S–Mo–S layer, lithium ions can easily intercalate/extract through MoS_2 layers. Thus, MoS_2 is a promising anode material and its capacity can be three and a half times that of commercial graphite anodes [9–13]. Reversible capacity as high as 1,290 mAh/g has been reported for the MoS_2-graphene composite electrode [14]. Compared to other emerging negative electrode materials, such as silicon or SnO_2, MoS_2 generally displays much better rate capability, lower cycling degradation, as well as low cost (e.g., sub-micro MoS_2 powder retails for dollars per kg) [15]. While silicon anodes possess an initial capacity around 3,500 mAh/g when tested at low rates (e.g., 0.1 C), they retain minimal capacity at high rates (e.g., 10 C) or after long term cycling due to their 280% volumetric expansion upon full lithiation and related unstable solid electrolyte interface [12]. In addition, nanostructured MoS_2 routinely outperforms its bulk equivalent in terms of capacity retention, rate capability, and cycle life, due to shorter lithium diffusion distances and higher concentrations of active edge sites, which further enhance their lithium storage capability [11, 16, 17].

However, electrodes based on layered MoS_2 do not work perfectly. Although the volume change of MoS_2 is significantly less than that in silicon-based electrodes, the theoretical 103% volume expansion via the conversion reaction of MoS_2 to Li_2S and molybdenum will still lead to depressed cycling stability and rate performance [18–21]. The intrinsically limited conductivity, restacking of MoS_2 nanosheets, side reactions between Li_2S and electrolyte, and polysulfide dissolution during cycling can further aggravate the degradation of electrochemical performance [22–24].

In order to ameliorate the electrical conductivity and structural stability of MoS_2 electrodes during cycling, carbonaceous materials, such as amorphous carbon, carbon fibers, porous carbon, carbon spheres, carbon nanotubes, and graphene, have been employed to form hybrid MoS_2-carbon systems [13, 25, 26]. The carbon component can enhance the electronic conductivity and concurrently buffer the volume changes of MoS_2 during the lithiation/delithiation reaction. At the same time, carbon materials can also act as a binder between the S/Li_2S and the molybdenum to prevent the loss of polysulfide during cycling [1, 23, 27, 28]. Based on these properties, hybrid MoS_2-carbon systems can lead to better electrode kinetics and more stable cycling performance [29–33].

Although some progress has been made in enhancing electrochemical performance by fabricating hybrid MoS_2/carbon electrode materials [34–36], there are still some challenges for this hybrid system. The restacking and aggregation of the nanocarbon materials, such as graphene or carbon nanotubes, or even MoS_2 nanomaterials during the fabrication process can lead to a serious loss of active surface area and sluggish ion transport kinetics. In addition, it is still difficult to coat or deposit a carbon layer with ideal thickness and compact contact interface onto nanosized MoS_2 materials. Thus, effectively controlling the carbon-coating process and avoiding the aggregation of the MoS_2/carbon is still a challenge.

Herein, we designed a two-layer carbon-coated MoS_2/carbon hybrid nanofiber material (MoS_2/C/C fiber), to serve as a high performance anode material for Li-ion batteries. Carbon-coated three-dimensional (3D) hierarchical MoS_2 nanospheres (MoS_2/C spheres) were fabricated first and then embedded into ~ 250 nm diameter electrospun fibers. The double-layer carbon coating plays a key role in preventing the aggregation of MoS_2 flakes, restraining the MoS_2 volume changes, and consumption of sulfides and molybdenum during lithiation/delithiation. Due to its structural stability and enhanced electron transport, the MoS_2/C/C fiber electrode manifests an outstanding reversible capacity and an excellent cycling performance. The double-layer carbon-coated MoS_2 composite electrode is a promising candidate anode active material for next generation lithium batteries with high capacity, high rate, and high cycling stability.

2 Experimental section

2.1 Preparation of MoS_2 spheres

In a typical reaction [2], 1 mmol hexaammonium heptamolybdate tetrahydrate ($(NH_4)_6Mo_7O_{24}\cdot4H_2O$, AR), 14 mmol thiourea (NH_2CSNH_2, ≥ 99.0%), and 0.01 mmol surfactant PVP (K32) were dissolved in 40 mL of deionized water (DI water) under vigorous stirring and ultrasonication for 30 min to form a homogeneous solution. Then, the solution was transferred into a 50 mL Teflon-lined stainless-steel autoclave and kept at 220 ℃ for 18 h. After being cooled to room temperature, the obtained precipitates were centrifuged and washed with DI water, acetone, and ethanol three times. The final products were dried at 70 °C under vacuum for 12 h.

2.2 Preparation of MoS_2/C spheres

In a typical synthesis [34], 100 mg of glucose and 200 mg of the above-obtained MoS_2 spheres were dissolved in 30 mL of DI water after violent stirring and ultrasonication for 30 min. Then, the solution was transferred into a 50 mL Teflon autoclave, followed by heating at 190 ℃ for 10 h. The autoclave was then cooled down to room temperature and the coating product was collected from the solution, washed with DI water and ethanol, and dried at 70 ℃ overnight. Finally, the produced powder was carbonized at 450 ℃ for 3 h under a nitrogen atmosphere to obtain the MoS_2/C spheres.

2.3 Preparation of MoS_2/C/C fiber

The mixture solution was prepared by adding 0.5 g of polyacrylonitrile (PAN) and 0.4 M of the above-obtained MoS_2/C spheres in 4.5 mL of N,N-dimethyl formamide (DMF). After stirring and ultrasonication for 30 min, the mixture solution was spun by a controlled electrospinning method. The applied working voltage, flow rate, and distance between the needle and the collector were fixed at 19 kV, 0.75 mL/h, and 15 cm, respectively. The electrospun fibers were collected from the aluminum foil and then prepared for further carbonization. In a typical carbonization process, the oxidative stabilization process was first carried out using a conventional muffle furnace at 280 ℃ for 1 h. Then, thermal treatment of the nanofiber film was performed at 1,000 ℃ for 3 h, with a continuous stable high-purity nitrogen gas.

2.4 Characterizations

X-ray diffraction (XRD) measurements were conducted with a Rigaku D/max 2550 V diffractometer using Cu Kα radiation at a wavelength of 1.5406 Å. Scanning electron microscopy (SEM) measurements were performed with a SU-8010 field emission SEM. Transmission electron microscopy (TEM), and elemental mapping were carried out using a FEI Tecnai G2 F20 TEM at 200 kV. X-ray photoelectron spectroscopy (XPS) measurements were performed using a Kratos Axis Ultra multi-functional X-ray photoelectron spectroscope with a typical detection depth of ~ 5 nm. All XPS spectra were corrected using the C 1s line at 284.7 eV. The carbon content of the samples was determined through thermogravimetric and differential scanning calorimetry (TG–DSC) using a Libra/209F1 with a speed of 10 ℃/min in ambient air in a temperature range of 50 to 700 ℃. Raman spectroscopy was performed using an inVia-Reflex with an excitation wavelength of 785 nm. Nitrogen adsorption and desorption isotherms at 77.3 K were carried out with an ASAP 2020 physisorption analyzer (USA).

2.5 Electrochemical measurements

2.5.1 Half-cell

The electrochemical properties of MoS_2 spheres, MoS_2/C spheres, and MoS_2/C/C fiber were investigated using a coin-type half-cell (CR2032). For the preparation of working electrodes, active materials, Super-P carbon black, and polyvinylidene fluoride (PVDF) with a mass ratio of 70:20:10 were mixed into a homogeneous slurry by adding DMF and the obtained slurry was pasted onto pure Cu foil and dried at 60 ℃ overnight. Lithium metal foil works as both counter and reference electrode. The cell used $LiPF_6$ (1 M) in ethylene carbonate/dimethyl carbonate/diethyl carbonate (1:1:1 vol.%) as the electrolyte and a Celgard 2400 polypropylene membrane as the separator. All the batteries were assembled in an argon-filled glovebox with humidity and oxygen levels lower than 1 ppm. The charge and discharge measurements of the cells

were performed on a LAND CT2001A electrochemical workstation between 0.005 and 3.00 V at room temperature. Cycling voltammogram (CV) tests of the batteries were performed by a CHI660D electrochemical workstation with the same potential range.

2.5.2 *Full-cell*

The MoS_2/C/C fiber electrode as active materials, Super-P carbon black, and PVDF with a mass ratio of 70:20:10 were mixed into a homogeneous slurry, which was then pasted onto pure copper foil as the anode electrode. The full cell was fabricated using a MoS_2/C/C fiber electrode on Cu foil as the anode, lithium cobalt oxide ($LiCoO_2$) on aluminum foil as the cathode electrode, with the same separator and electrolyte as in the half-cell. The charge and discharge measurements of the batteries were performed on a LAND CT2001A electrochemical workstation between 0.005 and 4.20 V. The average mass loading of the half-cell was 2.0–2.4 mg/cm^2. For the MoS_2/C/C/$LiCoO_2$ full cell, the mass loadings for the anode and cathode were 4.0 and 19.9 mg/cm^2, respectively.

3 Results and discussion

As illustrated in Fig. 1(a), the typical preparation process of MoS_2/C/C fiber hybrid electrodes consists of three steps, including one step for the MoS_2 spheres preparation and two steps for the double-layer carbon coating. In the first step, MoS_2 nanospheres were synthesized by a hydrothermal method. Then the prepared MoS_2 nanospheres were reacted with glucose and annealed under a N_2 atmosphere to get the first layer of the carbon coating. The typical morphologies of the MoS_2 and MoS_2/C nanospheres were characterized with SEM and TEM, as shown in Figs. 1(b) and 1(c) and Figs. S1 and S2 in the Electronic Supplementary Material (ESM). The pure MoS_2 exhibited similar spherical nanostructures with an average diameter of ~ 200 nm. The high resolution TEM images (Fig. S1 in the ESM) demonstrate that the MoS_2 flakes with lateral sizes of 50–100 nm and thicknesses of ~ 5 nm were highly interconnected and formed into a 3D nanosphere. The interconnected 3D structure can efficiently prevent the aggregation of MoS_2 nanosheets, ensuring electrode mechanical integrity. The MoS_2 nanosheets showed a typical lattice plane spacing of 0.66 nm for the (002) crystal plane, which exceeds the crystalline MoS_2 lattice spacing of 0.62 nm. The expanded spacing could decrease the energy barrier for Li ion intercalation. After being coated with the first carbon layer, the diameter of the MoS_2/C nanospheres increased by

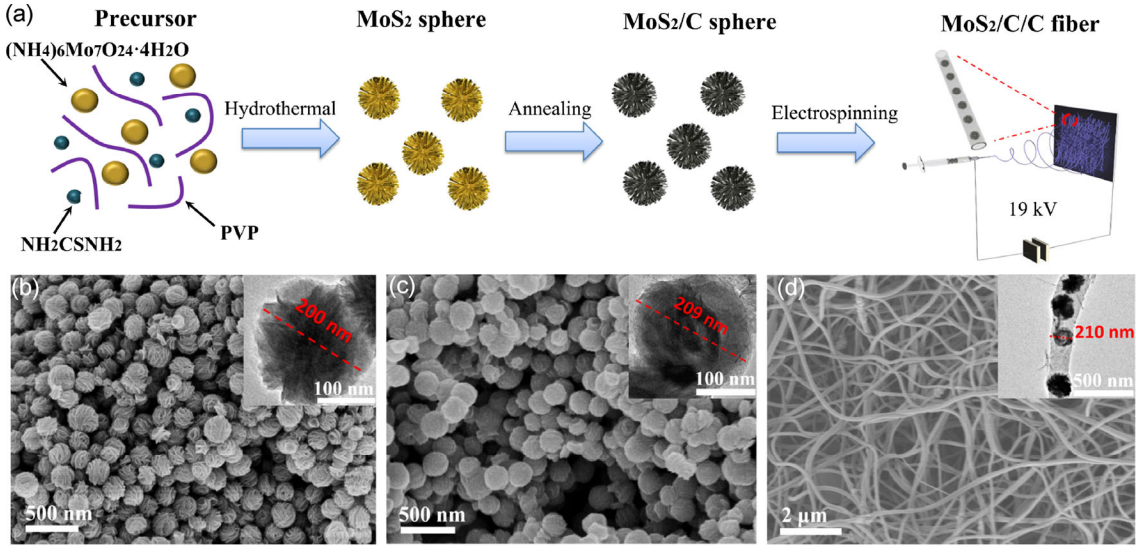

Figure 1 (a) Schematic illustration of the preparation process of MoS_2/C/C fiber electrodes. (b)–(d) SEM images of MoS_2 spheres, MoS_2/C spheres, and MoS_2/C/C fiber. The insets are the magnified TEM images of these three samples, respectively.

5–10 nm. As shown in the high resolution TEM image in Fig. S2 in the ESM, the very thin carbon layer was uniformly wrapped around the MoS_2 nanospheres without damaging the 3D network. The first carbon coating layer not only facilitates the intrinsic electron conductivity of the electrode material but also limits structural damage during the electrochemical process.

The MoS_2/C nanospheres were subsequently mixed with PAN and electrospun into nanofibers. As schematically illustrated in Fig. S3 in the ESM, the as-prepared nanofibers were pre-oxidized and then carbonized by high temperature thermal treatment. The as-prepared MoS_2/C/C fibers exhibited a homogeneous diameter distribution and smooth surface. As shown in the SEM image in Fig. 1(d), the diameters of the MoS_2/C/C fibers were mainly in the range of 250 to 280 nm. It is worth noting that no obvious MoS_2 nanosheets were found at the surface of the fibers, implying the embedding of MoS_2/C spheres inside the nanofibers. The low magnification TEM images in Figs. 2(a) and 2(b) clearly show the MoS_2/C spheres embedded into the carbon fiber networks. To further characterize the microstructure, we performed high-resolution TEM. A very clear two-layer carbon coating on MoS_2 spheres was observed. Furthermore, the high-resolution TEM energy dispersive spectroscopy (EDS) elemental mapping is shown in Figs. 2(e)–2(g), which exhibit the elemental distribution in the MoS_2/C/C fiber sample in the same region as that shown in Fig. 2(d). All of the molybdenum, sulfur,

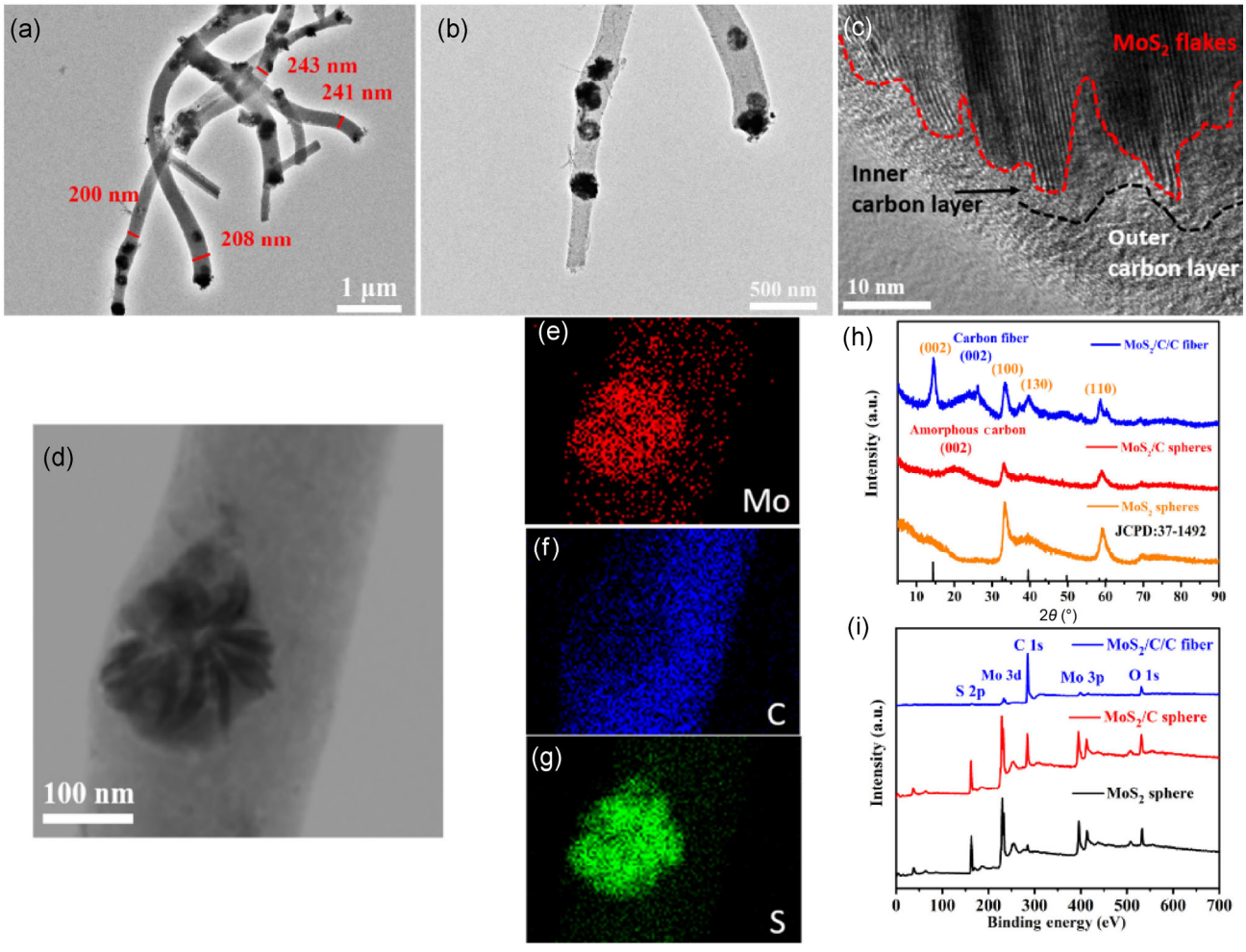

Figure 2 (a) and (b) TEM images of MoS_2/C/C fiber. (c) High-magnification TEM image corresponding to area of MoS_2/C/C fiber. (d)–(g) TEM images of MoS_2/C/C fiber electrode material and the corresponding elemental mapping images of Mo, S, and C. (h) XRD patterns of MoS_2, MoS_2/C, and MoS_2/C/C fiber. (i) The full range XPS spectra of MoS_2, MoS_2/C, and MoS_2/C/C fiber.

and carbon are distributed in specific regions of the 3D MoS_2/C/C fiber network, which further proves the successful preparation of the MoS_2/C/C fiber hybrid nanostructure.

The crystalline structure and chemical composition of the resultant MoS_2, MoS_2/C nanospheres, and MoS_2/C/C hybrid fiber were further studied by XRD and XPS. The XRD pattern of the MoS_2 nanospheres shows three dominant peaks of hexagonal crystalline 2H-MoS_2 (JCPDS: 37-1492). These three peaks, corresponding to the (002), (100), and (110) planes, emerge at 13.5°, 33.3°, and 58.9° [16], respectively. After thin layer carbon coating, the XRD pattern of the MoS_2/C spheres does not show any obvious changes from pure the MoS_2 spheres sample, except for the appearance of a broad peak at ~ 22° associated with amorphous carbon and a decrease in the intensity of the (100) plane peak of MoS_2, due to the thin layer carbon coating [36, 37]. For the XRD pattern of MoS_2/C/C fiber, the peak shown around 25° is ascribed to the outer layer carbon coating. The sharpened peaks corresponding to the (002) and (130) planes at 13.5° and 39.4°, respectively, are related to the high temperature thermal treatment and the shrinkage of the interlayer spacing of MoS_2 [38, 39].

XPS measurements were carried out to further clarify the components of these samples and the interfacial properties between MoS_2 flakes and the carbon layer. Overall, Fig. 2(i) shows the full XPS spectra of pure MoS_2, MoS_2/C, and MoS_2/C/C fiber materials. The spectrum from the pure MoS_2 spheres clearly exhibits peaks assigned to Mo 3d and 3p, S 2p, and O 1s. Both MoS_2/C and MoS_2/C/C fiber also include the C 1s peak, and the intensity ratio of C 1s for MoS_2/C/C fibers is much higher than that of MoS_2/C spheres.

The high-resolution XPS spectra of MoS_2, MoS_2/C nanospheres and MoS_2/C/C fibers are shown in Figs. S4–S6 in the ESM. Two peaks are observed at 228.6 and 231.9 eV, which can be attributed to the Mo $3d_{5/2}$ and Mo $3d_{3/2}$ binding energies, respectively, and are ascribed to the characteristic peaks of Mo^{4+} in MoS_2 flakes [40]. The peaks at 232.1 and 235.3 eV are related to the Mo $3d_{5/2}$ and $3d_{3/2}$ of Mo^{6+} (typical of the Mo–O–C bond) [26]. The peaks at 162.5 and 161.3 eV are attributed to the S $2p_{1/2}$ and S $2p_{3/2}$ peaks, which are related to the sulfur in MoS_2 [13]. The C 1s spectra can be decomposed into a dominant peak at 284.7 eV for C=C/C–C, and another broad peak related to oxygen-containing functional groups, which include C–O–Mo bonds [26]. The C–O–Mo bonds can be formed by bonding Mo atoms to oxygen-containing functional groups of the carbon precursor. The interfacial interaction of the C–O–Mo bond between MoS_2 and inner carbon layer should be beneficial for the electrochemical performance of the MoS_2/C/C fiber electrodes. As shown in Fig. S7 in the ESM, we further characterized the structure of MoS_2/C and MoS_2/C/C hybrid electrodes using Raman spectroscopy. For MoS_2/C, the two distinct peaks at 377 and 404 cm^{-1} correspond to the E^1_{2g} vibration mode (the in-plane displacement of Mo and S atoms) and the A_{1g} vibration mode (out-of-plane symmetric displacements of S atoms along the *c*-axis), respectively. After embedding MoS_2/C spheres into carbon fiber, these two MoS_2 related peaks disappeared due to the thick outer carbon layer. In addition, both MoS_2/C spheres and MoS_2/C/C fiber hybrid materials also displayed another two peaks at the bands around 1,360 (D band) and 1,590 (G band) cm^{-1}. The D band can be assigned to sp^3-hybridized disordered carbon or defective carbon, and the G band is associated with sp^2-hybridized graphitic carbon. The relative intensity ratio of I_D/I_G can roughly indicate the ratio of disordered carbon to graphitic carbon. The calculated values of I_D/I_G for MoS_2/C and MoS_2/C/C hybrid materials are 0.88 and 0.97, respectively, suggesting that MoS_2/C/C fiber contained a higher ratio of sp^3-hybridized carbon after the high temperature annealing. Figure S8 in the ESM reveals the thermogravimetric analysis of pure MoS_2, MoS_2/C spheres, and MoS_2/C/C fiber. The mass loss can be attributed to the decomposition of MoS_2 and carbon using Eqs. (1) and (2)

$$MoS_2 + O_2 \rightarrow MoO_3 + SO_2 \quad (1)$$

$$C + O_2 \rightarrow CO_2 \quad (2)$$

As shown in Fig. S8 in the ESM, in the case of pure MoS_2, 10% of the weight loss happened at approximately 350 °C owing to the oxidation of MoS_2 to MoO_3 under an air atmosphere. In contrast, MoS_2/C and MoS_2/C/C hybrid materials present a larger

weight loss of ~ 22% and 63%, respectively. The oxidative decomposition of carbon materials is thought to be the main reason for the different weight losses between MoS_2/C and MoS_2/C/C hybrid materials and pure MoS_2 material. Thus, the carbon contents in MoS_2/C and MoS_2/C/C hybrid materials are estimated to be 13.3% and 58.9%, respectively.

MoS_2, a well-known material, could offer some exciting electrochemical properties for lithium storage as an anode material. Intercalation of lithium into MoS_2 is known to occur within the voltage range of 0–3 V [13]. In the discharge process, a lithiation mechanism occurs at 1.1 V (vs. Li/Li$^+$) corresponding to Li$^+$ intercalation between the interlayers of MoS_2, forming Li_xMoS_2, which is fully reversible according to the reaction represented by Eq. (3)

$$MoS_2 + xLi^+ + xe^- \rightarrow Li_xMoS_2 \quad (3)$$

At voltages below 1.1 V vs. Li/Li$^+$, there appears to be a series of disproportionation reactions as well as the presence of intermediate metastable sulfide species [41]. Another dominant lithiation process at 0.3 V vs. Li/Li$^+$ is related to the transformation of Li_xMoS_2 into metallic Mo nanoparticles and Li_2S via a conversion reaction represented by Eq. (4)

$$Li_xMoS_2 + (4-x)Li^+ + (4-x)e^- \rightarrow Mo + 2Li_2S \quad (4)$$

The reaction of elemental sulfur and lithium at 2.2 V vs. Li/Li$^+$ can be described as in Eq. (5)

$$2Li^+ + S + 2e^- \rightarrow Li_2S \quad (5)$$

The theoretical specific capacity of the reaction from MoS_2 to Li_xMoS_2 (Eq. (3)) is 167 mAh/g, corresponding to the intercalation of one lithium ion per molybdenum atom. If the lithiation process goes deeper, attributed to the reversible conversion reaction of MoS_2 to Li_2S and metallic molybdenum as shown in Eq. (4), the theoretical specific charge capacity can reach up to 669 mAh/g. However, the reaction represented by Eq. (5) could yield a high theoretical capacity of 1,675 mAh/g, which is one of the reasons to produce MoS_2/carbon composites to achieve a high capacity over 1,000 mAh/g [42].

Based on the 3D network structure and double-layer carbon coating, MoS_2/C/C fiber could be a promising active material for high-performance energy storage. We systematically evaluated the electrochemical performance of a MoS_2/C/C fiber electrode as the anode of a Li-ion battery. Figure 3(a) shows the first three consecutive CV curves of the MoS_2/C/C fiber electrode with a scanning rate of 0.2 mV/s. In the first discharge process, a cathodic peak at 1.05 V (vs. Li/Li$^+$) corresponds to the reaction in Eq. (3). The peak at 0.42 V can be assigned to the transformation of Li_xMoS_2 into metallic Mo nanoparticles and Li_2S via a conversion reaction represented by Eq. (4). A wide shoulder peak emerges in the range of 0.6–0.8 V, which can be attributed to the formation of solid electrolyte interphase (SEI). The formation of an SEI layer can also make a significant contribution to the overall charge storage capacity [36, 43].

The intensities of these three peaks decreased in the following cycles. The two reduction peaks at 1.10 and 1.90 V can be attributed to formation of Li_xMoS_2 and Li_2S according to Eqs. (3) and (5). In the reverse anodic process, there are two oxidation peaks around 1.43 and 1.71 V, which are associated with the oxidation of Mo to Mo^{4+} and/or Mo^{6+} [15]. The dominant peak at 2.3 V could be assigned to the delithiation process of Li_2S

$$Li_2S \rightarrow 2Li^+ + S + 2e^- \quad (6)$$

These two peaks were in accordance with the peaks for pure MoS_2, providing further evidence of the charge storage origin. During the subsequent cycles, the reversible reaction is based on Eq. (7)

$$\begin{aligned} &\text{Lithiation:} \quad MoS_2 + 6Li^+ + S + 6e^- \rightarrow Mo + 3Li_2S \\ &\text{Delithiation:} \quad Li_2S \rightarrow 2Li^+ + S + 2e^- \end{aligned} \quad (7)$$

During subsequent discharge cycles, the obvious peak at 0.42 V almost disappeared while two new peaks were repeatedly observed at 1.9 and 1.1 V. These two peaks correspond to the conversion of S to polysulfides and then to Li_2S, which is consistent with other results in literature [44]. The oxidation peak at around 2.3 V, which is due to the oxidation of Li_2S to S and lithium ions [45, 46], is quite repeatable

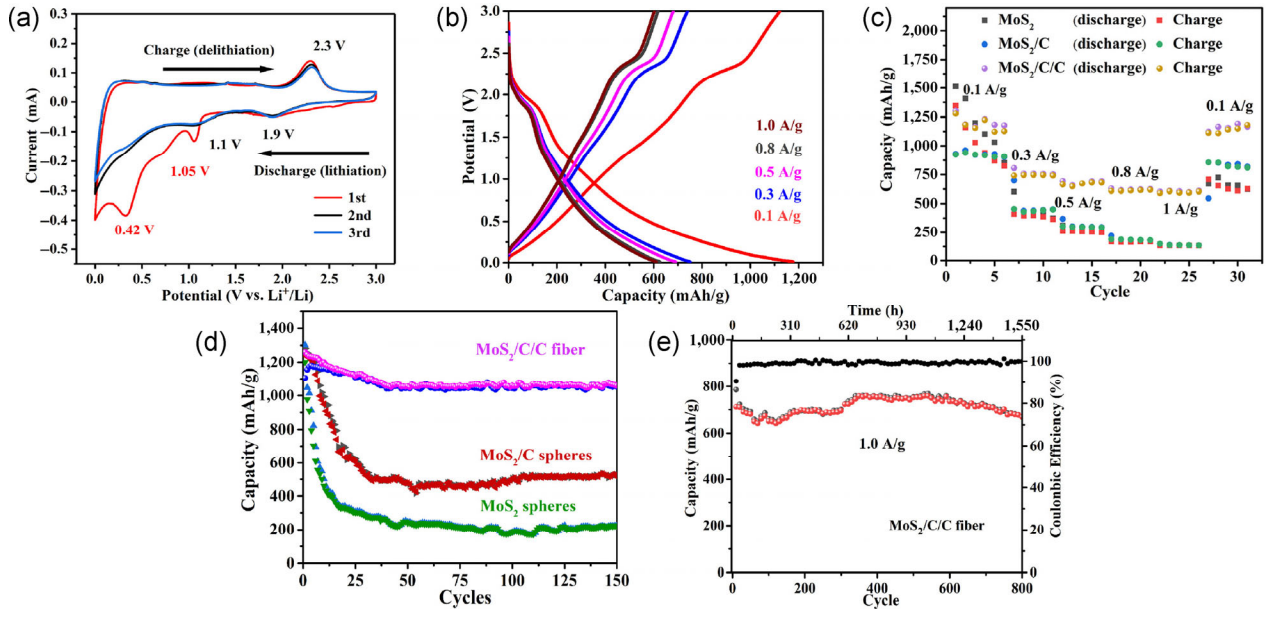

Figure 3 (a) CV of a MoS_2/C/C fiber electrode at a scanning rate of 0.2 mV/s during the initial three cycles. (b) The discharge/charge profiles of the MoS_2/C/C fiber electrode at different current densities. (c) Rate capability performance of the MoS_2, MoS_2/C, and MoS_2/C/C fiber electrodes. (d) Capacity retention of the MoS_2, MoS_2/C, and MoS_2/C/C fiber electrodes at a current density of 0.2 A/g for the subsequent 150 cycles. (e) Long-time cycling of the MoS_2/C/C fiber electrode at a current density of 1 A/g.

after the first cycle, indicating the good cycling stability of the MoS_2/C/C fiber hybrid electrode, as further revealed in the following electrochemical tests.

The specific capacity and rate capability of the MoS_2/C/C fiber electrode were tested by galvanostatic charge–discharge with different currents from 0.1 to 1.0 A/g. It is evident that the plateaus on the charge–discharge curves are consistent with the respective peaks on the CV curves. Similar charge and discharge plateau with different applied current densities revealed the good rate stability of the MoS_2/C/C fiber electrode. Figure 3(c) shows the superior rate capability of the MoS_2/C/C fiber electrode compared to that of pure MoS_2 spheres and MoS_2/C spheres electrodes. The measured reversible capacities of the MoS_2/C/C fiber electrode are 1301.2, 765.9, 680.8, 622.8, and 605.4 mAh/g at current densities of 0.1, 0.3, 0.5, 0.8, and 1.0 A/g, respectively. In contrast, the pure MoS_2 sphere electrode showed a rapid capacity drop with increasing current density. Although the rate capability of the MoS_2/C spheres electrode showed a minor improvement compared with pure MoS_2 sphere, it was still much lower than that of the double-layer carbon coated MoS_2/C/C fiber electrode. In addition, the rate capability of the MoS_2/C/C fiber electrode was higher than MoS_2/carbon nanotubes (500 mAh/g at 1 A/g) [23], carbon nanotube supported MoS_2 (300 mAh/g at 1 A/g) [47], and hierarchical MoS_2/polyaniline nanowires (330 mAh/g at 1 A/ g) [48].

The cycling performance of the MoS_2/C/C fiber electrode was evaluated at a current density of 0.2 A/g as shown in Fig. 3(d). The respective performance data for pure MoS_2 and MoS_2/C sphere electrodes were also included for comparison. The initial discharge capacities of pure MoS_2, MoS_2/C, and MoS_2/C/C fiber electrodes were 1,301, 1,281, and 1,275 mAh/g, respectively. The corresponding initial Coulombic efficiencies of these electrodes were 68.9%, 75.0%, and 85.0%. Such improved Coulombic efficiency can be related to the increased conductivity after double-layer carbon coating. The irreversible capacity loss during the initial few cycles is inevitable, because of the formation of the SEI layer [43, 49]. In the subsequent cycles, the Coulombic efficiency of the MoS_2/C/C fiber electrode gradually increased to 99.2%, superior to that of the MoS_2 and MoS_2/C electrodes with 93.3% and 98.2%, respectively. After 150 cycles, the MoS_2/C/C fiber electrode retained 83.3% (1,062 mAh/g) efficiency, which is much higher than the 40.9% (525 mAh/g) of

the MoS_2/C electrode and the 17.9% (234 mAh/g) of the pure MoS_2 electrode. Due to the direct exposure of MoS_2 to the electrolyte, it is inevitable to introduce the irreversible reaction of MoS_2 to dissoluble metallic Mo and Li_2S, which will lead to serious structure and electrochemistry fading during the charge and discharge process. Due to the partial blocking of this irreversible reaction, the cycling stability of MoS_2/C increased by over 20% after a thin layer of carbon coating. For the MoS_2/C/C electrode, the double-layer carbon coating could not only suppress the irreversible reaction, but also limit the volume change during the lithiation/delithiation process. In order to evaluate the long-term stability of the MoS_2/C/C fiber electrode, we ran the electrode with a high current density of 1 A/g for 800 cycles. After the long-term cycling, 92.6% of the initial charge capacity remained, which means only a 0.009% capacity loss per cycle. The Coulombic efficiency of the MoS_2/C/C fiber electrode reached 98.8% in the third cycle and stabilized between 98.8%–100% until the 800th cycle, illustrating its high Coulombic efficiency and cycling stability.

Based on the above discussion, the outstanding electrochemical properties of the MoS_2/C/C fiber electrode may be derived from the synergistic effects between the MoS_2 nanosphere network and the double-layer carbon coating. First, the introduction of the inner layer conductive carbon coating can prevent the restacking of MoS_2 nanosheets and increase the conductivity of the MoS_2 nanospheres, especially at the interface of MoS_2 nanosheets. Second, the robust outer layer carbon could effectively tolerate the volume change and prevent the loss of metallic molybdenum and sulfides during cycling. The conductive matrix of the carbon fiber can also provide a fast electron transport path for the whole electrode. Third, the fibrous network structure and high surface area of the MoS_2/C/C fiber electrode (371.6 m^2/g) also increased the area exposed to the electrolyte, facilitating ion diffusion and transport for high capacity and good rate capability (Fig. S9 in the ESM).

Figure 4 presents a schematic illustration showing

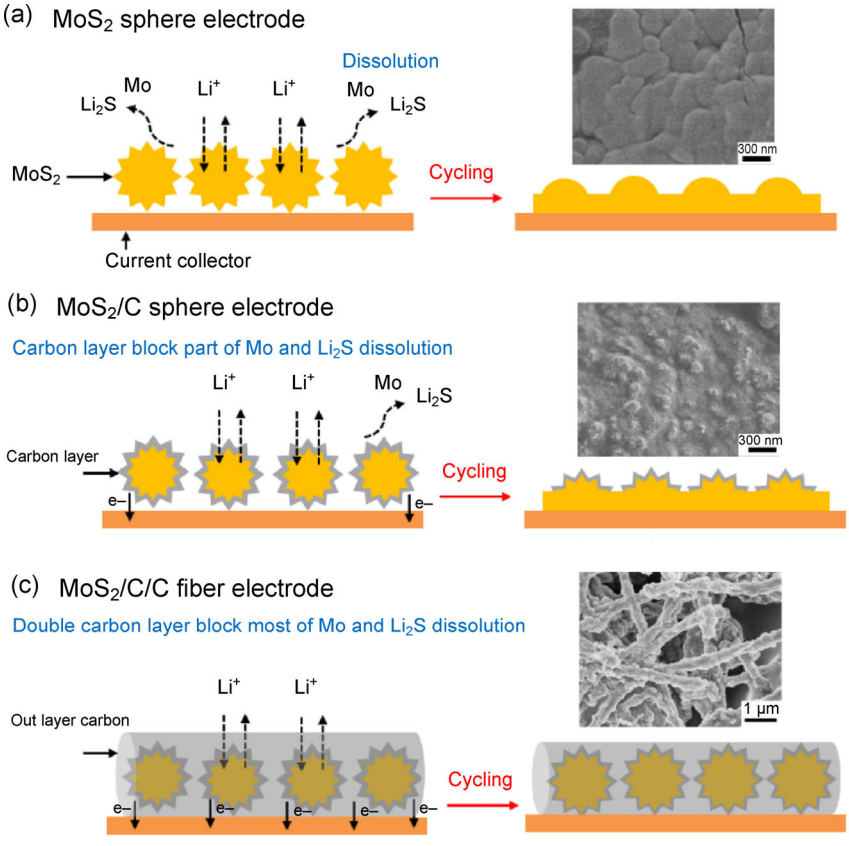

Figure 4 Schematic illustrating the lithiation process and the electrode structure fading and SEM images after 150 cycles of (a) pure MoS_2 sphere, (b) MoS_2/C spheres, and (c) MoS_2/C/C fiber.

the lithiation process and electrode structure evolution after long-term cycling. As demonstrated in the schematic and shown in SEM images, the pure MoS_2 spheres electrode showed serious structure fading and formed into continuous film after long-term cycling because of direct exposure of MoS_2 to the electrolyte [15, 27]. This could lead to the profound decomposition of MoS_2 nanospheres and the dissolution of metallic Mo and Li_2S. The MoS_2/C electrode also exhibited obvious structure change, but part of the nanosphere structures was still observed at the up surface of the electrode, due to the thin layer of carbon coating protection [34]. After coating with outer layer carbon fiber, the double-layer carbon coating could limit the volume change of the whole electrode and the dissolution of metallic Mo and sulfides during the lithiation/delithiation cycles. Thus, even after long-term cycling, the MoS_2/C/C fiber electrodes could still maintain the original fibrous network structure, which further explains why this double-layer carbon-coated MoS_2 material could display such an enhanced rate performance, high reversible capacity, and long-term cycle life [50].

To further demonstrate the promising properties of MoS_2/C/C fiber as the anode material of Li-ion batteries, we fabricated a full cell with a $LiCoO_2$ electrode as the cathode. Figure 5(a) indicates the working potential of $LiCoO_2$ is 3.0–4.2 V, while MoS_2/C/C shows a working potential of 0.0–3.0 V, which shows the great potential of these materials to form high performance full batteries and be used as the next general lithium-ion battery. Figure 5(b) exhibits the charge and discharge voltage profiles of the full battery, which show a potential from 0 to 4.2 V, a capacity of 155 mAh/g at 0.1 A/g, and close to the theoretical capacity of $LiCoO_2$. The total electrochemical reactions of the full cell can be explained by Eq. (8)

$$LiCoO_2 + xS + xMoS_2 \leftrightarrow 3xLi_2S + xMo + 6Li_{1-x}CoO_2 \quad (8)$$

A red LED was lit up for more than 60 min by the assembled full battery (Fig. 5(c)), which indicates great

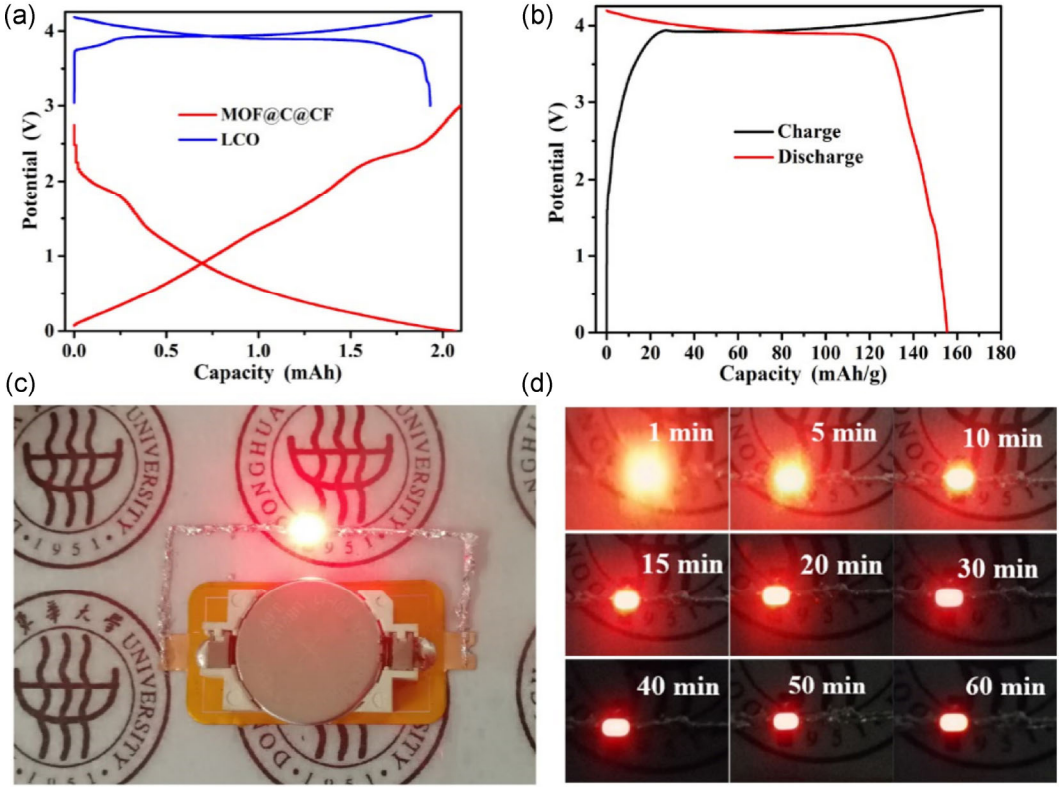

Figure 5 (a) Charge–discharge voltage profiles of MoS_2/C/C fiber and $LiCoO_2$ at 0.1 A/g. (b) Charge–discharge voltage profiles of a MoS_2/C/C//$LiCoO_2$ full battery at 0.1 A/g. (c) and (d) Red LEDs lit by the assembled full battery.

potential and practical application, and suggests the MoS_2/C/C fiber is a promising high-performance anode material. Figure S10 in the ESM shows the cycling performance of the MoS_2/C/C//$LiCoO_2$ full cell. The full cell retained 77% capacity after 80 cycles. After the initial 10 cycles, the capacity decreased to 107 mAh/g (83%) and the Coulombic efficiency stayed at 94%. However, the cell rapidly became more stable for the subsequent cycles, and achieved nearly 98% Coulombic efficiency for all following cycles.

4 Conclusions

In summary, we report a facile hydrothermal and subsequent electrospinning method to fabricate a double protective carbon layer coated MoS_2 fibrous electrode material, denoted as MoS_2/C/C fiber. Attributed to its intriguing double-layer carbon shell structure, the MoS_2/C/C fiber exhibits a series of remarkable electrochemical properties as the anode material of a Li-ion battery, such as a high first cycle specific capacity (1,275 mAh/g at 0.2 A/g), outstanding rate capability, and good capacity stability after long-term cycling (92.6% capacity retained after 800 cycles at 1 A/g). The high-energy storage performance of the MoS_2/C/C fiber material can be attributed to the design of the double carbon layer shell protection (inner amorphous carbon and outer carbon fiber). Furthermore, such a double-layer carbon coating strategy could prove useful in other areas of the energy storage field for improving rate capability and cycling stability.

Acknowledgements

We gratefully acknowledge the financial support by the National Natural Science Foundation of China (No. 51672043), the Natural Science Foundation of Shanghai (No. 15ZR1401200), Program for Professor of Special Appointment (Eastern Scholar) at Shanghai Institutions of Higher Learning, Program of Shanghai Academic Research Leader (No. 16XD1400100), Science and Technology Commission of Shanghai Municipality (No. 16JC1400700), Innovation Program of Shanghai Municipal Education Commission (No. 2017-01-07-00-03-E00055) and the Program of Introducing Talents of Discipline to Universities (No. 111-2-04). C. Y. H. thanks the Shanghai ChenGuang Program (No. 15CG33), the Natural Science Foundation of Shanghai (No. 16ZR1401500), and the Shanghai Sailing Program (No. 16YF1400400).

Electronic Supplementary Material: Supplementary material (additional information on bilayer $PdSe_2$ formed on monolayer graphene and bilayer graphene substrate, orientation of the nanoribbons on $PdSe_2$ islands) is available in the online version of this article at https://doi.org/10.1007/s12274-018-2096-7.

References

[1] Shan, T. T.; Xin, S.; You, Y.; Cong, H. P.; Yu, S. H.; Manthiram, A. Combining nitrogen-doped graphene sheets and MoS_2: A unique film–foam–film structure for enhanced lithium storage. *Angew. Chem.* **2016**, *128*, 12975–12980.

[2] Zhang, S. P.; Chowdari, B. V. R.; Wen, Z. Y.; Jin, J.; Yang, J. H. Constructing highly oriented configuration by few-layer MoS_2: Toward high-performance lithium-ion batteries and hydrogen evolution reactions. *ACS Nano* **2015**, *9*, 12464–12472.

[3] Hu, L. R.; Ren, Y. M.; Yang, H. X.; Xu, Q. Fabrication of 3D hierarchical MoS_2/polyaniline and MoS_2/C architectures for lithium-ion battery applications. *ACS Appl. Mater. Interfaces* **2014**, *6*, 14644–14652.

[4] Chang, K.; Chen, W. X. L-cysteine-assisted synthesis of layered MoS_2/graphene composites with excellent electrochemical performances for lithium ion batteries. *ACS Nano* **2011**, *5*, 4720–4728.

[5] Xiao, J.; Wang, X. J.; Yang, X. Q.; Xun, S. D.; Liu, G.; Koech, P. K.; Liu, J.; Lemmon, J. P. Electrochemically induced high capacity displacement reaction of PEO/MoS_2/graphene nanocomposites with lithium. *Adv. Funct. Mater.* **2011**, *21*, 2840–2846.

[6] Liu, H.; Su, D. W.; Zhou, R. F.; Sun, B.; Wang, G. X.; Qiao, S. Z. Highly ordered mesoporous MoS_2 with expanded spacing of the (002) crystal plane for ultrafast lithium ion

storage. *Adv. Energy Mater*. **2012**, *2*, 970–975.

[7] Eda, G.; Yamaguchi, H.; Voiry, D.; Fujita, T.; Chen, M. W.; Chhowalla, M. Photoluminescence from chemically exfoliated MoS_2. *Nano Lett.* **2011**, *11*, 5111–5116.

[8] Wei, W.; Sun, K.; Hu, Y. H. An efficient counter electrode material for dye-sensitized solar cells—Flower-structured 1T metallic phase MoS_2. *J. Mater. Chem. A* **2016**, *4*, 12398–12401.

[9] Xiao, J.; Choi, D.; Cosimbescu, L.; Koech, P.; Liu, J.; Lemmon, J. P. Exfoliated MoS_2 nanocomposite as an anode material for lithium ion batteries. *Chem. Mater.* **2010**, *22*, 4522–4524.

[10] Shao, Y. L.; Li, J. M.; Li, Y. G.; Wang, H. Z.; Zhang, Q. H.; Kaner, R. B. Flexible quasi-solid-state planar micro-supercapacitor based on cellular graphene films. *Mater. Horiz.* **2017**, *4*, 1145–1150.

[11] Li, J. H.; Shao, Y. L.; Shi, Q. W.; Hou, C. Y.; Zhang, Q. H.; Li, Y. G.; Kaner, R. B.; Wang, H. Z. Calligraphy-inspired brush written foldable supercapacitors. *Nano Energy* **2017**, *38*, 428–437.

[12] Chan, C. K.; Peng, H. L.; Liu, G.; McIlwrath, K.; Zhang, X. F.; Huggins, R. A.; Cui, Y. High-performance lithium battery anodes using silicon nanowires. *Nat. Nanotechnol*. **2008**, *3*, 31–35.

[13] Zhou, J. W.; Qin, J.; Zhang, X.; Shi, C. S.; Liu, E. Z.; Li, J. J.; Zhao, N. Q.; He, C. N. 2D space-confined synthesis of few-layer MoS_2 anchored on carbon nanosheet for lithium-ion battery anode. *ACS Nano* **2015**, *9*, 3837–3848.

[14] Chang, K.; Chen, W. X. *In situ* synthesis of MoS_2/graphene nanosheet composites with extraordinarily high electrochemical performance for lithium ion batteries. *Chem. Commun.* **2011**, *47*, 4252–4254.

[15] Stephenson, T.; Li, Z.; Olsen, B.; Mitlin, D. Lithium ion battery applications of molybdenum disulfide (MoS_2) nano-composites. *Energy Environ. Sci.* **2014**, *7*, 209–231.

[16] Wang, T. Y.; Chen, S. Q.; Pang, H.; Xue, H. G.; Yu, Y. MoS_2-based nanocomposites for electrochemical energy storage. *Adv. Sci*. **2017**, *4*, 1600289.

[17] Chang, K.; Chen, W. X. Single-layer MoS_2/graphene dispersed in amorphous carbon: Towards high electrochemical performances in rechargeable lithium ion batteries. *J. Mater. Chem.* **2011**, *21*, 17175–17184.

[18] Xu, X.; Fan, Z. Y.; Yu, X. Y.; Ding, S. J.; Yu, D. M.; Lou, X. W. D. A nanosheets-on-channel architecture constructed from MoS_2 and CMK-3 for high-capacity and long-cycle-life lithium storage. *Adv. Energy Mate*. **2014**, *4*, 1400902.

[19] Shu, H. B.; Li, F.; Hu, C. L.; Liang, P.; Cao, D.; Chen, X. S. The capacity fading mechanism and improvement of cycling stability in MoS_2-based anode materials for lithium-ion batteries. *Nanoscale* **2016**, *8*, 2918–2926.

[20] Wu, H.; Lou, Z.; Yang, H.; Shen, G. Z. A flexible spiral-type supercapacitor based on $ZnCo_2O_4$ nanorod electrodes. *Nanoscale* **2015**, *7*, 1921–1926.

[21] Wu, H.; Jiang, K.; Gu, S. S.; Yang, H.; Lou, Z.; Chen, D.; Shen, G. Z. Two-dimensional $Ni(OH)_2$ nanoplates for flexible on-chip microsupercapacitors. *Nano Res*. **2015**, *8*, 3544–3552.

[22] Zhu, C. B.; Mu, X. K.; van Aken, P. A.; Yu, Y.; Maier, J. Single-layered ultrasmall nanoplates of MoS_2 embedded in carbon nanofibers with excellent electrochemical performance for lithium and sodium storage. *Angew. Chem., Int. Ed.* **2014**, *53*, 2152–2156.

[23] Zhang, C. F.; Wang, Z. Y.; Guo, Z. P.; Lou, X. W. Synthesis of MoS_2-C one-dimensional nanostructures with improved lithium storage properties. *ACS Appl. Mater. Interfaces* **2012**, *4*, 3765–3768.

[24] Li, Z. Y.; Ottmann, A.; Zhang, T.; Sun, Q.; Meyer, H. P.; Vaynzof, Y.; Xiang, J. H.; Klingeler, R. Preparation of hierarchical C@MoS_2@C sandwiched hollow spheres for lithium ion batteries. *J. Mater. Chem. A* **2017**, *5*, 3987–3994.

[25] Ma, L.; Ye, J. B.; Chen, W. X.; Chen, D. Y.; Lee, J. Y. Gemini surfactant assisted hydrothermal synthesis of nanotile-like MoS_2/graphene hybrid with enhanced lithium storage performance. *Nano Energy* **2014**, *10*, 144–152.

[26] Wang, Y.; Chen, B.; Seo, D. H.; Han, Z. J.; Wong, J. I.; Ostrikov, K.; Zhang, H.; Yang, H. Y. MoS_2-coated vertical graphene nanosheet for high-performance rechargeable lithium-ion batteries and hydrogen production. *NPG Asia Mater*. **2016**, *8*, e268.

[27] Chen, B.; Liu, E. Z.; Cao, T. T.; He, F.; Shi, C. S.; He, C. N.; Ma, L. Y.; Li, Q. Y.; Li, J. J.; Zhao, N. Q. Controllable graphene incorporation and defect engineering in MoS_2-TiO_2 based composites: Towards high-performance lithium-ion batteries anode materials. *Nano Energy* **2017**, *33*, 247–256.

[28] Zhou, X. S.; Wan, L. J.; Guo, Y. G. Facile synthesis of MoS_2@CMK-3 nanocomposite as an improved anode material for lithium-ion batteries. *Nanoscale* **2012**, *4*, 5868–5871.

[29] Yu, X. Y.; Hu, H.; Wang, Y. W.; Chen, H. Y.; Lou, X. W. Ultrathin MoS_2 nanosheets supported on N-doped carbon nanoboxes with enhanced lithium storage and electrocatalytic properties. *Angew. Chem., Int. Ed*. **2015**, *54*, 7395–7398.

[30] Shao, Y. L.; Wang, H. Z.; Zhang, Q. H.; Li, Y. G. Fabrication of large-area and high-crystallinity photoreduced graphene oxide films via reconstructed two-dimensional multilayer structures. *NPG Asia Mater*. **2014**, *6*, e119.

[31] Shao, Y. L.; El-Kady, M. F.; Lin, C. W.; Zhu, G. Z.; Marsh, K. L.; Wang, J. Y.; Zhang, Q. H.; Li, Y. G.; Wang, H. Z.; Kaner, R. B. 3D freeze-casting of cellular graphene films

for ultrahigh-power-density supercapacitors. *Adv. Mater.* **2016**, *28*, 6719–6726.

[32] Shi, Q. W.; Li, J. H.; Hou, C. Y.; Shao, Y. L.; Zhang, Q. H.; Li, Y. G.; Wang, H. Z. A remote controllable fiber-type near-infrared light-responsive actuator. *Chem. Commun.* **2017**, *53*, 11118–11121.

[33] Li, K. R.; Shao, Y. L.; Liu, S. Y.; Zhang, Q. H.; Wang, H. Z.; Li, Y. G.; Kaner, R. B. Aluminum-ion-intercalation supercapacitors with ultrahigh areal capacitance and highly enhanced cycling stability: Power supply for flexible electrochromic devices. *Small* **2017**, *13*, 1700380.

[34] Zhu, C. B.; Mu, X. K.; van Aken, P. A.; Maier, J.; Yu, Y. Fast Li storage in MoS_2-graphene-carbon nanotube nanocomposites: Advantageous functional integration of 0D, 1D, and 2D nanostructures. *Adv. Energy Mater.* **2015**, *5*, 1401170.

[35] Chen, B.; Lu, H. H.; Zhou, J. W.; Ye, C.; Shi, C. S.; Zhao, N. Q.; Qiao, S. Z. Porous MoS_2/carbon spheres anchored on 3D interconnected multiwall carbon nanotube networks for ultrafast Na storage. *Adv. Energy Mater.* **2018**, 201702909.

[36] Gong, Y.; Yang, S.; Zhan, L.; Ma, L.; Vajtai, R.; Ajayan, P. M. A bottom-up approach to build 3D architectures from nanosheets for superior lithium storage. *Adv. Funct. Mater.* **2014**, *24*, 125–130.

[37] Ng, S. H.; Wang, J. Z.; Wexler, D.; Konstantinov, K.; Guo, Z. P.; Liu, H. K. Highly reversible lithium storage in spheroidal carbon-coated silicon nanocomposites as anodes for lithium-ion batteries. *Angew. Chem., Int. Ed.* **2006**, *45*, 6896–6899.

[38] Wang, L.; Yu, Y.; Chen, P. C.; Zhang, D. W.; Chen, C. H. Electrospinning synthesis of C/Fe_3O_4 composite nanofibers and their application for high performance lithium-ion batteries. *J. Power Sources* **2008**, *183*, 717–723.

[39] Toprakci, O.; Ji, L. W.; Lin, Z.; Toprakci, H. A. K.; Zhang, X. W. Fabrication and electrochemical characteristics of electrospun $LiFePO_4$/carbon composite fibers for lithium-ion batteries. *J. Power Sources* **2011**, *196*, 7692–7699.

[40] Xiong, X. Q.; Lou, W.; Hu, X. L.; Chen, C. J.; Qie, L.; Hou, D. F.; Huang, Y. H. Flexible membranes of MoS_2/C nanofibers by electrospinning as binder-free anodes for high-performance sodium-ion batteries. *Sci. Rep*. **2015**, *5*, 9254.

[41] He, P. G.; Zhao, K. R.; Huang, B. Y.; Zhang, B. Q.; Huang, Q.; Chen, T. F.; Zhang, Q. Q. Mechanically robust and size-controlled MoS_2/graphene hybrid aerogels as high-performance anodes for lithium-ion batteries. *J. Mater. Sci.* **2018**, *53*, 4482–4493.

[42] Chen, C.; Xie, X. Q.; Anasori, B.; Sarycheva, A.; Makaryan, T.; Zhao, M. Q.; Urbankowski, P.; Miao, L.; Jiang, J. J.; Gogotsi, Y. MoS_2-on-MXene heterostructures as highly reversible anode materials for lithium-ion batteries. *Angew. Chem.* **2018**, *130*, 1864–1868.

[43] Sun, Y. M.; Liu, N.; Cui, Y. Promises and challenges of nanomaterials for lithium-based rechargeable batteries. *Nat. Energy* **2016**, *1*, 16071.

[44] Hwang, H.; Kim, H.; Cho, J. MoS_2 nanoplates consisting of disordered graphene-like layers for high rate lithium battery anode materials. *Nano Lett.* **2011**, *11*, 4826–4830.

[45] Wang, J.; Liu, J. L.; Chao, D. L.; Yan, J. X.; Lin, J. Y.; Shen, Z. X. Self-assembly of honeycomb-like MoS_2 nanoarchitectures anchored into graphene foam for enhanced lithium-ion storage. *Adv. Mater.* **2014**, *26*, 7162–7169.

[46] Xiong, F. Y.; Cai, Z. Y.; Qu, L. B.; Zhang, P. F.; Yuan, Z. F.; Asare, O. K.; Xu, W. W.; Lin, C.; Mai, L. Q. Three-dimensional crumpled reduced graphene oxide/MoS_2 nanoflowers: A stable anode for lithium-ion batteries. *ACS Appl. Mater. Interfaces* **2015**, *7*, 12625–12630.

[47] Shi, Y. M.; Wang, Y.; Wong, J. I.; Tan, A. Y. S.; Hsu, C. L.; Li, L. J.; Lu, Y. C.; Yang, H. Y. Self-assembly of hierarchical MoS_x/CNT nanocomposites ($2 < x < 3$): Towards high performance anode materials for lithium ion batteries. *Sci. Rep.* **2013**, *3*, 2169.

[48] Yang, L. C.; Wang, S. N.; Mao, J. J.; Deng, J. W.; Gao, Q. S.; Tang, Y.; Schmidt, O. G. Hierarchical MoS_2/polyaniline nanowires with excellent electrochemical performance for lithium-ion batteries. *Adv. Mater.* **2013**, *8*, 1180–1184.

[49] Armstrong, A. R.; Lyness, C.; Panchmatia, P. M.; Islam, M. S.; Bruce, P. G. The lithium intercalation process in the low-voltage lithium battery anode $Li_{1+x}V_{1-x}O_2$. *Nat. Mater.* **2011**, *10*, 223–229.

[50] Wu, S. P.; Xu, R.; Lu, M. J.; Ge, R. Y.; Iocozzia, J.; Han, C. P.; Jiang, B. B.; Lin, Z. Q. Graphene-containing nanomaterials for lithium-ion batteries. *Adv. Energy Mater.* **2015**, *5*, 1500400.